P. Flores[1]
Departamento de Engenharia Mecânica,
Universidade do Minho,
Campus de Azurém,
4800-058 Guimarães Portugal
e-mail: pflores@dem.uminho.pt

J. Ambrósio
Instituto de Engenharia Mecânica (IDMEC),
Instituto Superior Técnico,
Av. Rovisco Pais 1,
1049-001 Lisboa Portugal
e-mail: jorge@dem.ist.utl.pt

J. C. P. Claro
Departamento de Engenharia Mecânica,
Universidade do Minho,
Campus de Azurém,
4800-058 Guimarães Portugal
e-mail: jcpclaro@dem.uminho.pt

H. M. Lankarani
Department of Mechanical Engineering,
Wichita State University,
Wichita, KS 67260
e-mail: hamid.lankarani@wichita.edu

Dynamics of Multibody Systems With Spherical Clearance Joints

This work deals with a methodology to assess the influence of the spherical clearance joints in spatial multibody systems. The methodology is based on the Cartesian coordinates, with the dynamics of the joint elements modeled as impacting bodies and controlled by contact forces. The impacts and contacts are described by a continuous contact force model that accounts for geometric and mechanical characteristics of the contacting surfaces. The contact force is evaluated as function of the elastic pseudo-penetration between the impacting bodies, coupled with a nonlinear viscous-elastic factor representing the energy dissipation during the impact process. A spatial four-bar mechanism is used as an illustrative example and some numerical results are presented, with the efficiency of the developed methodology discussed in the process of their presentation. The results obtained show that the inclusion of clearance joints in the modelization of spatial multibody systems significantly influences the prediction of components' position and drastically increases the peaks in acceleration and reaction moments at the joints. Moreover, the system's response clearly tends to be nonperiodic when a clearance joint is included in the simulation. [DOI: 10.1115/1.2198877]

Keywords: clearance joints, multibody dynamics

Introduction

In recent years, the influence of clearance joints on the dynamics of multibody systems has been the topic for many research activities [1–4]. Several researchers have devoted special attention to planar systems [5,6]. However, the utility of the methodologies developed is somewhat restricted because they are not valid for spatial multibody systems such as vehicle models, car suspensions, and robotic manipulators, where the system motion is not limited to be planar. In fact, even planar systems may exhibit out-of-plane motion due to misalignments, thus justifying the development of mathematical models to assess the influence of the clearance joints in spatial multibody systems. Clearances at different joints of mechanical systems are known as sources for impact forces, resulting in wear and tear of the joint. The impacts within the clearances of machines are transmitted throughout the multibody system, which can seriously degrade their performance. The evolution of the contact forces are of paramount importance in the analysis and design of mechanical systems with clearance joints [3–6].

The present work deals with a methodology to assess the influence of the spherical clearance joints in spatial multibody systems that are composed by rigid bodies connected by kinematic joints. When there is a clearance in a spherical joint, impacts between the socket and the ball can occur, and consequently, local deformations take place. The impact is internal and the response of the system is performed using a continuous contact force model. The normal force is evaluated as a function of the elastic pseudo-penetration between the impacting bodies, coupled with a nonlinear viscous-elastic factor representing the energy dissipation dur-

ing the impact process [7]. The collision between the joints elements is known as an impact during which forces are developed that act and disappear over a short period of time. The duration of the contact period governs the choice of the method used to analyze the impact. The type of energy dissipation governs the modeling of the contact-impact force [7–9]. Thus, in modeling a spherical clearance joint, the three kinematic constraints associated with the ideal joints are removed and three extra degrees of freedom are introduced instead. The dynamics of the joint is then controlled by forces developed on the socket and ball. While an ideal spherical joint in a multibody system imposes kinematic constraints, a spherical clearance joint leads to force constraints.

A detailed discussion of the results relative to a spatial four-bar mechanism simulation, which include a spherical joint with clearance, is presented.

Modeling Spherical Joints With Clearance

In this section, a mathematical model of a spherical joint with clearance in spatial multibody systems is presented. In standard multibody models, it is assumed that the connecting points of two bodies, linked by an ideal spherical joint, are coincident. The introduction of the clearance in a spherical joint separates these two points and the bodies become free to move relative to each other. Consequently, the three kinematic constraints associated with the ideal joint are removed and three relative degrees of freedom are allowed instead. Thus, a spherical joint with clearance does not constrain any degree of freedom from the system like the ideal spherical joint. In a spherical clearance joint, the dynamics of the joint is controlled by contact-impact forces that result from the collision between the bodies connected. Thus, these types of joints can be referred to as force joints, since they deal with force constraints instead of kinematic constraints.

Figure 1 depicts two bodies i and j connected by a spherical joint with clearance. A spherical part of body j, the ball, is inside of a spherical part of body i, the socket. The radii of socket and ball are R_i and R_j, respectively. The difference in radius between the socket and the ball defines the radial clearance: $c = R_i - R_j$. The
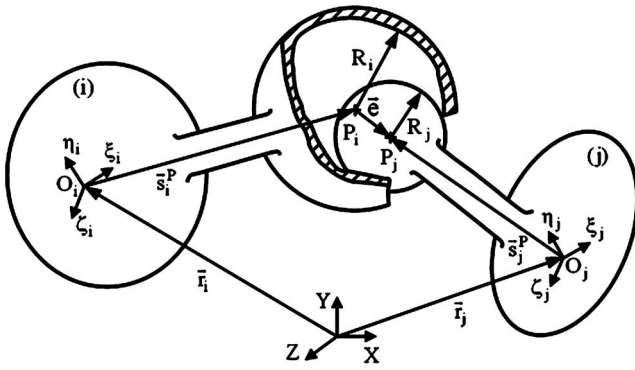
Fig. 1 Spherical joint with clearance in a multibody system

Fig. 2 Penetration between the socket and the ball

center of mass of bodies i and j are O_i and O_j, respectively. Body-fixed coordinate systems $\xi\eta\zeta$ are attached at their center of mass, while XYZ represents the global coordinate system. Point P_i indicates the center of the socket, being the center of the ball denoted by P_j. The vector that connects the point P_i to point P_j is defined as the eccentricity vector $\mathbf{e}$, as shown in Fig. 1. Note that, in real mechanisms, the magnitude of the eccentricity is typically much smaller than the radius of the socket and ball.

As displayed in Fig. 1, the eccentricity vector $\mathbf{e}$, which connects the centers of the socket and the ball, is given by

$$\mathbf{e} = \mathbf{r}_j^P - \mathbf{r}_i^P \tag{1}$$

where both $\mathbf{r}_j^P$ and $\mathbf{r}_i^P$ are described in global coordinates with respect to the inertial reference frame [10]

$$\mathbf{r}_k^P = \mathbf{r}_k + \mathbf{A}_k \mathbf{s}_k'^P, \quad (k=i,j) \tag{2}$$

where $\mathbf{A}_i$ is the transformation matrix and $\mathbf{s}_k'^P$ is the local position vector of point P. The magnitude of the eccentricity vector is evaluated as

$$e = \sqrt{\mathbf{e}^T\mathbf{e}} \tag{3}$$

where $\mathbf{e}^T$ is the transpose of vector $\mathbf{e}$. The magnitude of the eccentricity vector expressed in the global coordinates is written as

$$e = \sqrt{(x_j^P - x_i^P)^2 + (y_j^P - y_i^P)^2 + (z_j^P - z_i^P)^2} \tag{4}$$

and the rate of change of the eccentricity in the radial direction, that is, in the direction of the line of centers of the socket and the ball is

$$\dot{e} = \frac{(x_j^P - x_i^P)(\dot{x}_j^P - \dot{x}_i^P) + (y_j^P - y_i^P)(\dot{y}_j^P - \dot{y}_i^P) + (z_j^P - z_i^P)(\dot{z}_j^P - \dot{z}_i^P)}{e} \tag{5}$$

in which the dot denotes the derivative with respect to time.

A unit vector $\mathbf{n}$ normal to the collision surface between the socket and the ball is aligned with the eccentricity vector, as can be observed in Fig. 2. Therefore,

$$\mathbf{n} = \frac{\mathbf{e}}{e} \tag{6}$$

Figure 2 illustrates the situation in which the socket and the ball bodies are in contact, which is identified by the existence of a relative penetration. The contact or control points on bodies i and j are Q_i and Q_j, respectively. The global position of the contact points in the socket and ball are given by

$$\mathbf{r}_k^Q = \mathbf{r}_k + \mathbf{A}_k \mathbf{s}_k'^Q + R_k \mathbf{n}, \quad (k=i,j) \tag{7}$$

where R_i and R_j are the socket and ball radii, respectively.

The velocity of the contact points Q_i and Q_j in the global coordinate system is obtained by differentiating Eq. (7) with respect to time, yielding
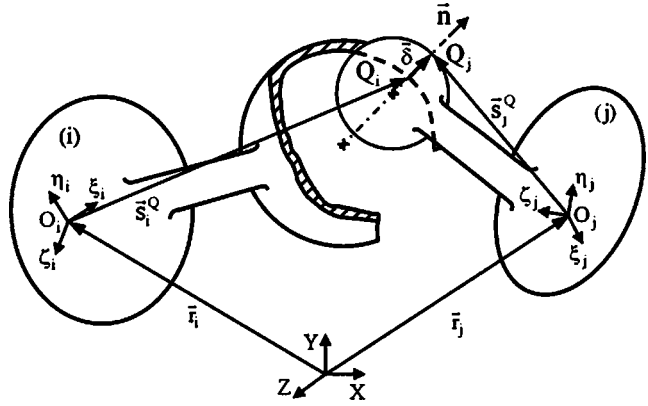
$$\dot{\mathbf{r}}_k^Q = \dot{\mathbf{r}}_k + \dot{\mathbf{A}}_k \mathbf{s}_k'^Q + R_k \dot{\mathbf{n}}, \quad (k=i,j) \tag{8}$$

where $\dot{\mathbf{n}}$ is evaluated by differentiating Eq. (6).

Let the components of the relative velocity of contact points in the normal and tangential direction to the surface of collision be represented by $\mathbf{v}_N$ and $\mathbf{v}_T$, respectively. The relative normal velocity determines whether the contact bodies are approaching or separating, and the relative tangential velocity determines whether the contact bodies are sliding or sticking. The relative scalar velocities, normal and tangential to the surface of collision, are obtained by projecting the relative impact velocity onto the tangential and normal directions

$$\mathbf{v}_N = [(\dot{\mathbf{r}}_j^Q - \dot{\mathbf{r}}_i^Q)^T \mathbf{n}]\mathbf{n} \tag{9}$$

$$\mathbf{v}_T = (\dot{\mathbf{r}}_j^Q - \dot{\mathbf{r}}_i^Q)^T - \mathbf{v}_N \equiv v_T \mathbf{t} \tag{10}$$

where $\mathbf{t}$ represents the tangential direction to the impacted surfaces. It is assumed that there is no contact between the ball and the opening area in the socket.

Observing Fig. 2, it is clear that the geometric condition for contact between the socket and ball can be defined as

$$\delta = e - c \tag{11}$$

where e is the magnitude of the eccentricity vector given by Eq. (3) and c is the radial clearance. It should be noted that here the clearance is taken as a specified parameter. When the magnitude of the eccentricity vector is smaller than the radial clearance there is no contact between the socket and the ball and, consequently, they can freely move relative to each other. When the magnitude of eccentricity is larger than radial clearance, there is contact between the socket and ball, being the relative penetration given by Eq. (11). Then a constitutive contact law, such as the continuous contact force model proposed by Lankarani and Nikravesh [7], is applied in order to evaluate the contact force developed in the direction perpendicular to the plane of collision. Thus, the module of the contact force, or joint reaction force, can be written as

$$\begin{cases} F_N = 0, & \text{if } \delta < 0 \\ F_N \neq 0, & \text{if } \delta > 0 \end{cases} \tag{12}$$

The normal and tangential force vectors at the contact points, which result from the contact, are represented by $\mathbf{f}_N$ and $\mathbf{f}_T$, respectively. Since these forces do not act through the center of mass of the bodies i and j, the moment components for each body need to be evaluated. Furthermore, the contribution of the contact forces to the generalized vector of forces are found by projecting the normal and tangential forces onto the X, Y, and Z directions. Based on Fig. 3, the equivalent forces and moments working on the center of mass of body i are given by

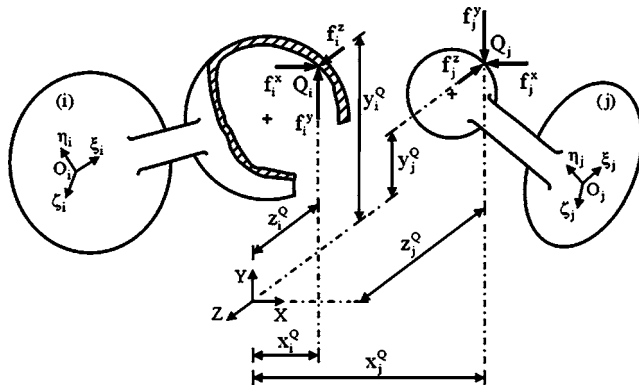$$\mathbf{f}_i = \mathbf{f}_N + \mathbf{f}_T \tag{13}$$

Fig. 3 Contact forces defined at the points of contact between socket and ball

$$\mathbf{m}_i = \tilde{\mathbf{s}}_i^Q \mathbf{f}_i \qquad (14)$$

where a tilde ($\sim$) placed over a vector indicates that the components of the vector are used to generate a skew-symmetric matrix [10].

The forces and moments acting on body j are written as

$$\mathbf{f}_j = -\mathbf{f}_i \qquad (15)$$

$$\mathbf{m}_j = -\tilde{\mathbf{s}}_j^Q \mathbf{f}_i \qquad (16)$$

Modes of the Ball Motion Inside the Socket

When some amount of clearance is included in a spherical joint, the ball and socket can move relative to each other. Figure 4 illustrates the different possible types of ball motion inside the socket; namely: contact or following mode, free flight mode, and impact mode. In the contact or following mode, the ball and the socket are in permanent contact and a rolling or sliding motion relative to each other exists. This mode ends when the ball and socket separate from each other and the ball enters in free flight mode. In the free flight motion, the ball moves freely inside the socket boundaries, that is, the ball and the socket are not in contact, hence there is no joint reaction force. In the impact mode, which occurs at the termination of the free flight motion, impact forces are applied to the system. This mode is characterized by an abrupt discontinuity in the kinematic and dynamic responses, and a significant exchange of momentum occurs between the two impacting bodies is observed. At the termination of the impact mode, the ball can enter either in free flight or in the following mode. During the dynamic simulation of a spherical joint with clearance, if the path of the socket center is plotted for each instant, the
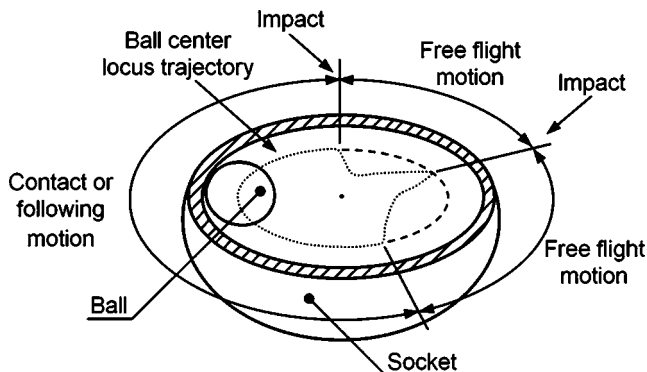

Fig. 4 Modes of the ball motion inside the socket

different modes of motion of the socket inside the ball can easily be observed. The stiction between ball and socket is not considered in the present work.

Contact Force Model

Impact, such as it happens in a spherical clearance joint, is one of the most common types of dynamic loading conditions that give rise to impulsive forces, which in turn excite higher vibration modes and affect the dynamic characteristics of the mechanical systems. Thus, for a spherical joint with clearance, the contact between the socket and the ball can be modeled by the well known Hertz contact law [11]

$$F_N = K\delta^n \qquad (17)$$

where K is the stiffness coefficient and δ is the relative penetration. The exponent n is set to 1.5. The parameter K depends on the material and geometric properties of the contacting surfaces. For two spherical surfaces in contact, the generalized stiffness parameter is given by [9]

$$K = \frac{4}{3(\sigma_i + \sigma_j)} \left[\frac{R_i R_j}{R_i + R_j} \right]^{1/2} \qquad (18)$$

where the material parameters σ_i and σ_j are given by

$$\sigma_k = \frac{1 - \nu_k^2}{E_k}, \quad (k = i, j) \qquad (19)$$

and ν_k and E_k are the Poisson's ratio and the Young's modulus associated with each sphere, respectively.

The Hertz contact law given by Eq. (18) is a pure elastic model; that is, it does not include any energy dissipation. Lankarani and Nikravesh [7] extended the Hertz contact law to include energy loss due to internal damping as

$$F_N = K\delta^n \left[1 + \frac{3(1 - c_e^2)}{4} \frac{\dot{\delta}}{\dot{\delta}^{(-)}} \right] \qquad (20)$$

where the stiffness coefficient K can be evaluated by Eqs. (18) and (19), c_e is the restitution coefficient, $\dot{\delta}$ is the relative penetration velocity, and $\dot{\delta}^{(-)}$ is the initial impact velocity.

Equation (20) is only valid for impact velocities lower than the propagation speed of elastic waves across the bodies [7]. This criterion is fulfilled in the applications used this work. While, the clearance joints are designed to operate at high speed mechanical systems. However, with low values of clearance size, the impact velocities in the joint are within a tolerable range of validity of the contact force model given by Eq. (20) [6,8].

The force expressed by Eq. (20), when drawn versus penetration, results in a hysteresis loop as shown in Fig. 5. The area of this hysteresis loop is equal to the energy loss due to the internal damping of the material. The hysteresis damping function assumes that the loss in energy during impact is due to the material damping of the colliding bodies, which dissipates energy in the form of heat [7].

Multibody Systems Formulation

This section presents a brief revision of the formulation of the general multibody mechanical systems. The methodology presented was implemented in the computer program DAP-3D, which has been developed for the spatial dynamic analysis of general multibody systems [10]. Due to its simplicity and computational easiness, Cartesian coordinates are used to formulate the dynamics of the spatial multibody systems. In this approach, the equations of motion can easily be assembled automatically by the computer package.

Let Fig. 6 represent a rigid body i to which a body-fixed coordinate system $(\xi\eta\zeta)_i$ is attached at its center of mass.
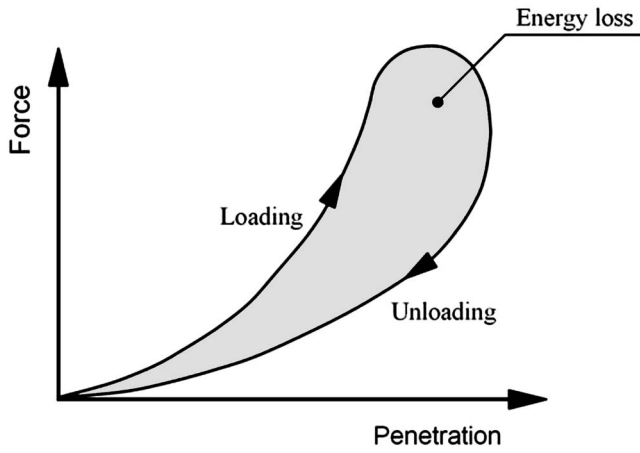
Fig. 5   Force versus penetration

When Cartesian coordinates are used, the position and orientation of the rigid body must be defined by a set of translational and rotational coordinates. The position of the body with respect to global coordinate system XYZ is defined by the coordinate vector $\mathbf{r}_i = [xyz]_i^T$ that represents the localization of the local reference frame $(\xi\eta\zeta)_i$. The orientation of the body is described by the rotational coordinate's vector $\mathbf{p}_i = [e_0 e_1 e_2 e_3]_i^T$, which includes the Euler parameters for the rigid body [10]. Therefore, the vector of coordinates that describes completely the rigid body i is

$$\mathbf{q}_i = [\mathbf{r}_i^T \ \mathbf{p}_i^T]_i^T \tag{21}$$

According to this definition, a spatial multibody system with nb bodies is described by a set of coordinates $\mathbf{q}$ in the form

$$\mathbf{q}_i = [\mathbf{q}_1^T, \mathbf{q}_2^T, \ldots, \mathbf{q}_{nb}^T]_i^T \tag{22}$$

A point P on body i can be defined by position vector $\mathbf{s}_i^P$, which represents the location of point P with respect to the body-fixed reference frame $(\xi\eta\zeta)_i$, and by the global position vector $\mathbf{r}_i$; that is,

$$\mathbf{r}_i^P = \mathbf{r}_i + \mathbf{s}_i^P = \mathbf{r}_i + \mathbf{A}_i \mathbf{s}_i'^P \tag{23}$$

where $\mathbf{A}_i$ is the transformation matrix for body i that defines the orientation of the referential $(\xi\eta\zeta)_i$ with respect to the referential frame XYZ. The transformation matrix is expressed as function of the four Euler parameters as [10]
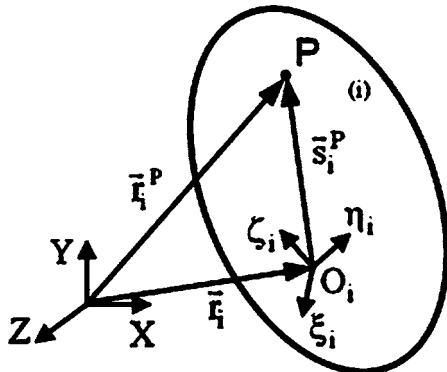

Fig. 6   Rigid body in Cartesian coordinates

$$\mathbf{A}_i = \begin{bmatrix} e_0^2 + e_1^2 - \dfrac{1}{2} & e_1 e_2 - e_0 e_3 & e_1 e_3 + e_0 e_2 \\[2mm] e_1 e_2 + e_0 e_3 & e_0^2 + e_2^2 - \dfrac{1}{2} & e_2 e_3 - e_0 e_1 \\[2mm] e_1 e_3 - e_0 e_2 & e_2 e_3 + e_0 e_1 & e_0^2 + e_3^2 - \dfrac{1}{2} \end{bmatrix}_i \tag{24}$$

Notice that the vector $\mathbf{s}_i^P$ is expressed in global coordinates whereas the vector $\mathbf{s}_i'^P$ is defined in the body i fixed coordinate system. Throughout the formulation presented in this work, the quantities with $(\cdot)'$ means that $(\cdot)$ is expressed in local system coordinates.

The velocities and accelerations of body i use the angular velocities $\boldsymbol{\omega}_i'$ and accelerations $\dot{\boldsymbol{\omega}}_i'$ instead of the time derivatives of the Euler parameters, which simplifies the mathematical formulation and do not have critical singular cases [12]. When Euler parameters are employed as rotational coordinates, the relation between their time derivatives $\dot{\mathbf{p}}_i$ and the angular velocities is expressed by [10]

$$\dot{\mathbf{p}}_i = \frac{1}{2} \mathbf{L}^T \boldsymbol{\omega}_i' \tag{25}$$

where the auxiliary matrix $\mathbf{L}$ is function of Euler parameters

$$\mathbf{L}_i = \begin{bmatrix} -e_1 & e_0 & e_3 & -e_2 \\ -e_2 & -e_3 & e_0 & e_1 \\ -e_3 & e_2 & -e_1 & e_0 \end{bmatrix}_i \tag{26}$$

The velocities and accelerations of body i are given by vectors

$$\dot{\mathbf{q}}_i^* = [\dot{\mathbf{r}}_i^T \ \boldsymbol{\omega}_i'^T]_i^T \tag{27}$$

$$\ddot{\mathbf{q}}_i^* = [\ddot{\mathbf{r}}_i^T \ \dot{\boldsymbol{\omega}}_i'^T]_i^T \tag{28}$$

Multibody Systems' Equations of Motion

In terms of the Cartesian coordinates, the equations of motion of an unconstrained multibody mechanical system are written as

$$\mathbf{M}\ddot{\mathbf{q}} = \mathbf{g} \tag{29}$$

where $\mathbf{M}$ is the global mass matrix, containing the mass and moment of inertia of all bodies and $\mathbf{g}$ is a force vector that contains the external and Coriolis forces acting on the bodies of the system. For a constrained multibody system, the kinematical joints are described by a set of holonomic algebraic constraints denoted as

$$\boldsymbol{\Phi}(\mathbf{q}, t) = \mathbf{0} \tag{30}$$

Using the Lagrange multipliers technique the constraints are added to the equations of motion. These are written together with the second time derivative of the constraint equations. Thus, the set of equations that describe the motion of the multibody system is

$$\begin{bmatrix} \mathbf{M} & \boldsymbol{\Phi}_q^T \\ \boldsymbol{\Phi}_q & \mathbf{0} \end{bmatrix} \begin{Bmatrix} \ddot{\mathbf{q}}^* \\ \boldsymbol{\lambda} \end{Bmatrix} = \begin{Bmatrix} \mathbf{g} \\ \boldsymbol{\gamma} \end{Bmatrix} \tag{31}$$

where $\boldsymbol{\lambda}$ is the vector of Lagrange multipliers and $\boldsymbol{\gamma}$ is the vector that groups all the terms of the acceleration constraint equations that depend on the velocities only; that is

$$\boldsymbol{\gamma} = -(\boldsymbol{\Phi}_q \dot{\mathbf{q}})_q \dot{\mathbf{q}} - \boldsymbol{\Phi}_{tt} - 2\boldsymbol{\Phi}_{qt}\dot{\mathbf{q}} \tag{32}$$

Equation (31) is a differential algebraic equation that has to be solved, being the resulting accelerations integrated in time. However, because Eq. (31) does not use explicitly the position and velocity constraint equations, there is no insurance that the system constraints are not violated during the forward dynamic solution process. To avoid constraints violation during numerical integration, the Baumgarte stabilization technique is used; i.e., Eq. (31) is modified to
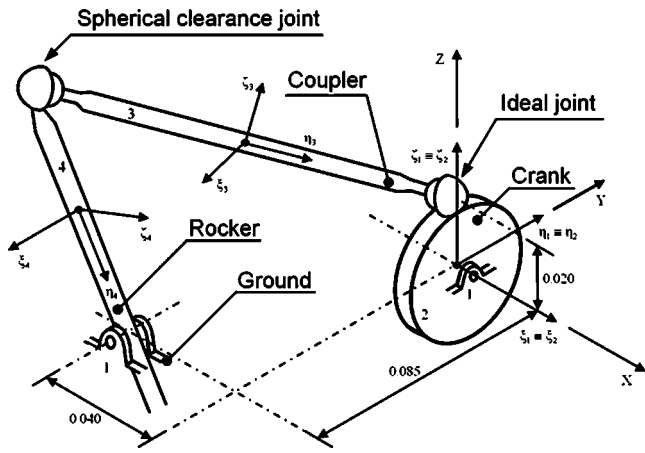
Fig. 7 Spatial four bar mechanism which includes a spherical clearance joint between the coupler and rocker

$$\begin{bmatrix} \mathbf{M} & \mathbf{\Phi_q}^T \\ \mathbf{\Phi_q} & \mathbf{0} \end{bmatrix} \begin{Bmatrix} \ddot{\mathbf{q}} \\ \boldsymbol{\lambda} \end{Bmatrix} = \begin{Bmatrix} \mathbf{g} \\ \boldsymbol{\gamma} - 2\alpha\dot{\mathbf{\Phi}} - \beta^2\mathbf{\Phi} \end{Bmatrix} \qquad (33)$$

where α and β are positive constants that represent the feedback control parameters for the velocity and position constraint violations [10,13].

According to the formulation outlined, the dynamic response of multibody systems involves the evaluation of the Jacobian matrix $\mathbf{\Phi}_q$ and of the vectors $\mathbf{g}$ and $\boldsymbol{\gamma}$, for each time step. The following step is to solve Eq. (33) to obtain the system accelerations $\ddot{\mathbf{q}}$. These accelerations, together with the velocities $\dot{\mathbf{q}}^*$, are integrated in order to obtain the new velocities $\dot{\mathbf{q}}$ and positions $\mathbf{q}^*$ for the next time step. This process is repeated until the complete description of system's motion is obtained for the selected time interval. In this description it should be noted that, in vector $\dot{\mathbf{q}}^*$, the angular velocities are substituted by the time derivatives of the Euler parameters, using Eq. (25).

The numerical integration method used is a predictor-corrector algorithm with both variable order and step size [14], which converts the second-order differential equations into first-order equations by defining auxiliary vectors.

Example Application

In this section the application to the four bar mechanism that describes a spatial motion is employed, as an illustrative example to demonstrate how a spherical clearance joint can affect the behavior of the mechanism. The spatial four bar mechanism consists of four rigid bodies that represent the ground, crank, coupler and rocker. The body numbers and their corresponding local coordinate systems are shown in Fig. 7.

The kinematic joints of this multibody system include two ideal revolute joints, connecting the ground to the crank and the ground to the rocker, and one perfect spherical joint that connects the crank and coupler. A spherical joint, with a given clearance, interconnects the coupler and rocker. This four-bar mechanism is modeled with 28 coordinates, which result from the four rigid bodies,

Table 1 Geometric and inertia properties of the spatial four-bar mechanism.

Body No.	Length [m]	Mass [kg]	Moment of inertia [Kg m²]		
			$I_{\xi\xi}$	$I_{\eta\eta}$	$I_{\zeta\zeta}$
2	0.020	0.0196	0.0000392	0.0000197	0.0000197
3	0.122	0.1416	0.0017743	0.0000351	0.0017743
4	0.074	0.0316	0.0001456	0.0000029	0.0001456

Table 2 Simulation parameters for the four-bar mechanism.

Joint socket radius	10.0 mm
Joint ball radius	9.5 mm
Restitution coefficient	0.9
Young's modulus	207 GPa
Poisson's ratio	0.3
Baumgarte coefficient α	5
Baumgarte coefficient β	5
Integration time step	0.00001 s
Integration tolerance	0.000001 s

four Euler parameter normalization constraints, and nineteen kinematic constraints. Consequently, this system has five degrees of freedom.

The initial configuration of the spatial four bar mechanism is illustrated in Fig. 7. The system is released from the initial position with null velocities and under the action of gravity force, which is taken to act in the negative Z-direction. Thus, the heights of centers of mass of all bodies dominate the total potential system energy and control the dynamic system's behavior.

The dimensions and inertia properties of each body are in Table 1. The dynamic parameters, used for the simulation and for the numerical methods required to solve the system dynamics, are listed in Table 2.

In order to study the influence of the spherical clearance model in the global behavior of the spatial four bar mechanism, some kinematic and dynamic characteristics, corresponding to the first two seconds of the simulation, are presented and discussed in what follows. The results are compared to those obtained with a simulation in which all kinematic joints are considered to be ideal or perfect.

The normal contact force and the joint reaction force, for the first impact at the spherical clearance joint, are shown in Fig. 8. The plotted reaction force is the magnitude of the force in the revolute joint that connects the ground to the rocker. The simulation is performed by using the Lankarani and Nikravesh contact force model given by Eq. (20).

By observing Fig. 8, it is clear how the impacts inherent to dynamics of the clearance joint influence the reaction force. The two force curves plotted show a very similar shape. The maximum reaction force is about 60% of the contact force.

Figure 9 shows the hysteresis curves for the first three impacts at the spherical clearance joint. The contact force decreases for each impact suggesting that some system energy is dissipated from impact to impact. This dissipated energy is measured as the area enclosed by the hysteresis plot. The energy dissipation is logical since the gravitational force is the only external action,
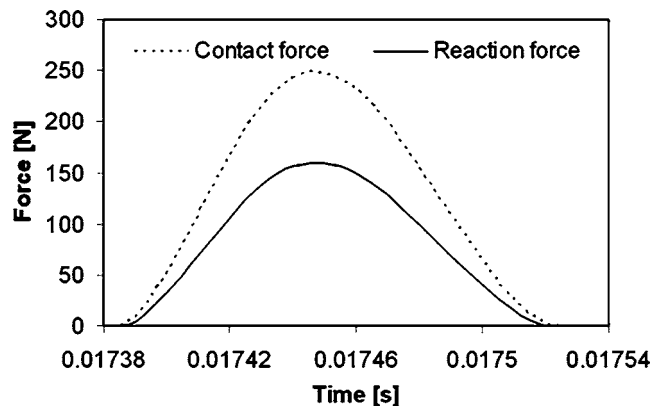

Fig. 8 Normal contact force at the clearance joint and corresponding reaction force in the ground-rocker revolute joint for the first impact
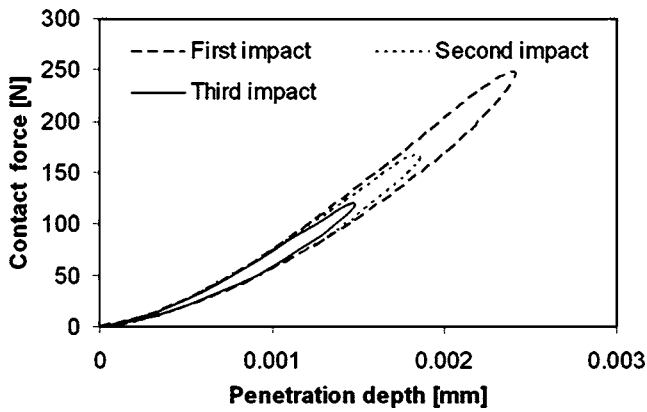
Fig. 9 Hysteresis loop of the first three impacts at the clearance joint. The contact force decreases from impact to impact because no energy is feed to the system.

that is, in this simulation no other external forces or drivers were applied to the system, meaning that no energy was feed to the system.

Figures 10–13 depict the Z-component for the position, velocity and acceleration of the center of mass of rocker, as well as the Y-component of the reaction moment that acts at the revolute joint that connects the ground to the rocker, for both ideal and spherical clearance joint simulations. The results plotted in Fig. 10 show that the position accuracy of the four-bar mechanism is clearly influenced by the effect joint clearance. Furthermore, the maximum Z-position is not reached in every cycle since the impacts within the joint with clearance dissipate some of the system's
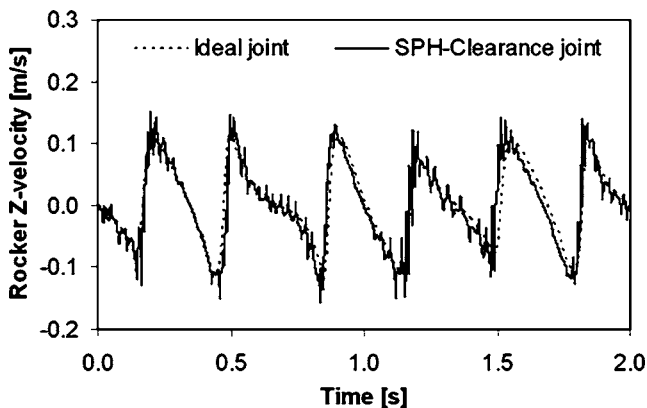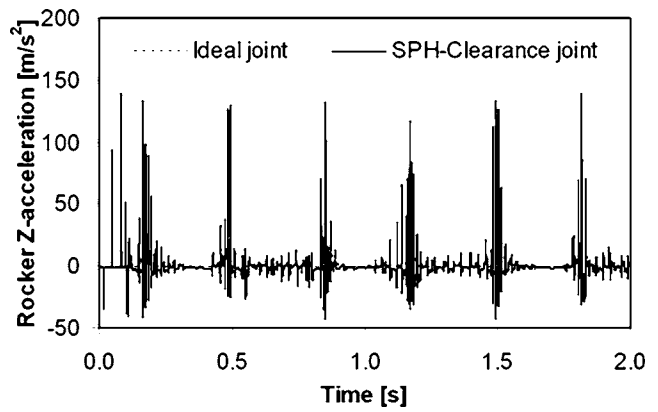

Fig. 12 Z-acceleration of rocker center of mass

energy. Figures 12 and 13 show that the mechanism with clearance joint creates significantly larger dynamic accelerations and reaction moments on the system than those observed for an ideal dynamic model. The level of acceleration and moment for the case of the ideal joint is very low (not visible in the figures) since there was no driver in the system, with the gravitational force the only external action on the system.

The magnitude of the eccentricity vector is plotted in Fig. 14, in which the different types of motion between the ball center and the socket center can be observed; namely, free flight, impact, rebound, and permanent or continuous contact. In the first instants of the simulation, free flight motion followed by impacts and rebounds are well evident. After that, it can be observed that the ball
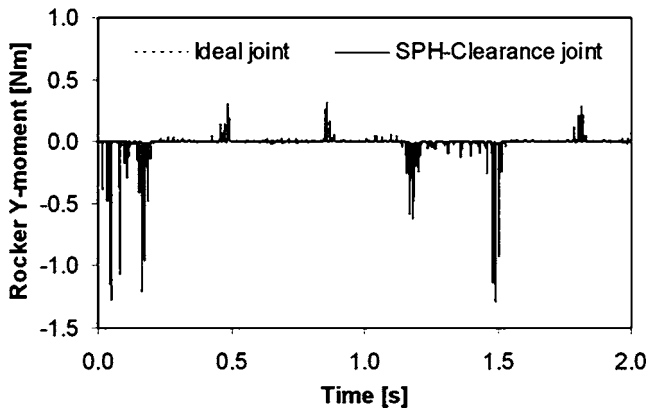

Fig. 10 Z-coordinate of rocker center of mass

Fig. 13 Y-component of the reaction moment at the ground-rocker revolute joint

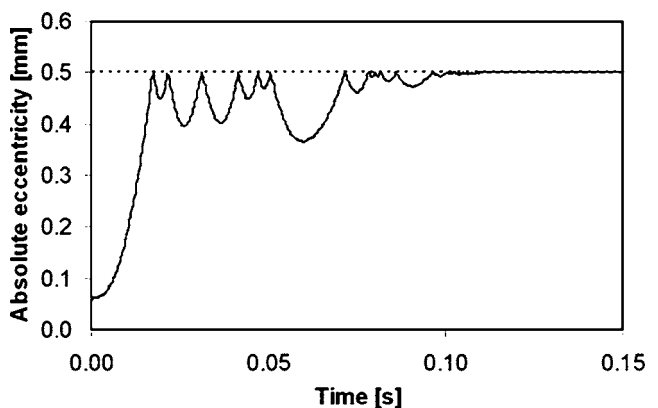**Fig. 11 Z-velocity of rocker center of mass**
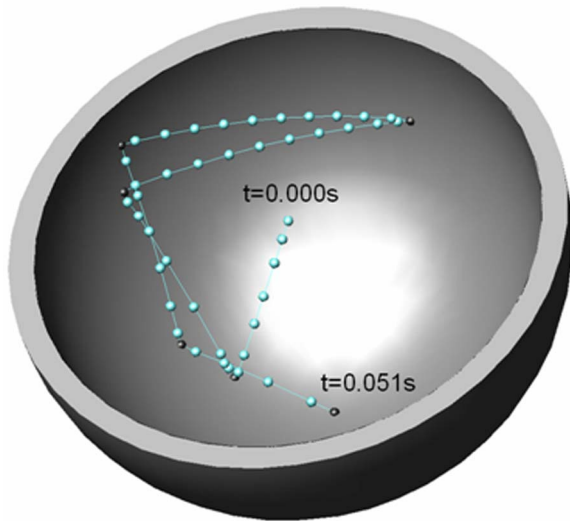

Fig. 14 Module of the eccentricity vector

Fig. 15 First simulation's instants in which free flight motion and impacts followed by rebounds are visible

and socket present periods of permanent or continuous contact, where the socket follows the ball wall. The dashed line in Fig. 14 represents the radial clearance size (0.5 mm), which corresponds to the maximum relative motion between the ball and socket without contact.

The path of the socket center relative to the ball center is also illustrated in Figs. 15 and 16. Figure 15 shows the relative motion between the two bodies for the first six impacts. The inner spherical surface represents the clearance limit while the small spheres inside represent the ball center path. The free flights are illustrated by clear spheres, whereas the impacts are represented by darker spheres. It is clear that in the first instants of simulation the impacts are immediately followed by rebounds. Figure 16 shows the time interval simulation from 0.100 to 0.150 s. From this figure, it is observed that the socket is always in permanent contact with the ball wall. Furthermore, the permanent contact between the ball and socket is accomplished by varying penetration depth along the radial direction.

The Poincaré maps are used to illustrate the dynamic behavior of the spatial four bar mechanism with a spherical clearance joint.
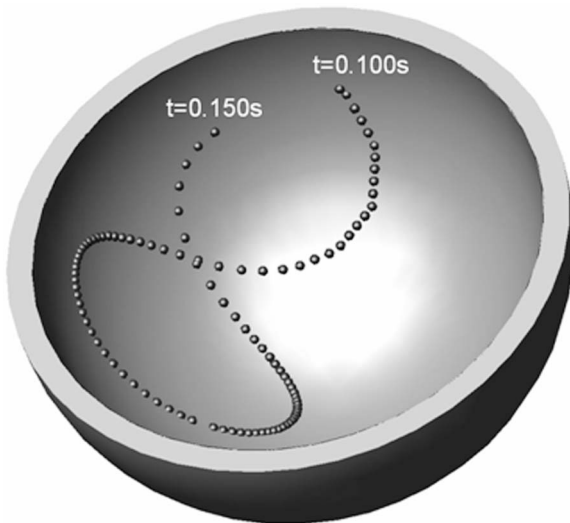

Fig. 16 Ball center trajectory inside the socket. Permanent or continuous contact, i.e., the ball follows the socket wall.
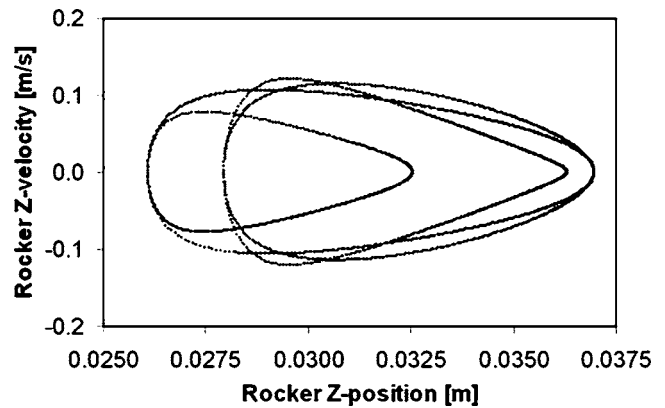
Fig. 17 Poincaré map: ideal joint

The system's response is nonlinear, as the relative motion between the ball and socket can change from free flights, impact, and continuous contact, as it is illustrated in Figs. 15 and 16. This nonlinear system response is well visible by plotting the corresponding Poincaré maps, which relates the rocker Z-velocity versus rocker Z-position, shown in Figs. 17 and 18. The Poincaré map presented in Fig. 18 has a complex aspect, densely filled by orbits or points, which indicates chaotic behavior. Even for the ideal joint case, the system's response is not periodic since the closed orbits in the Poincaré map do not repeat from cycle to cycle.

Conclusions

This work has been presented a general methodology to analyze the kinematic and dynamic characteristics of spatial multibody systems with spherical clearance joints.

This methodology is based on the Cartesian coordinates, the joint elements are modeled as impacting bodies and the dynamics of the joints is controlled by contact-impact forces. These impacts and contacts are described by a continuous contact force model that takes into account the geometric and mechanical characteristics of the contacting surfaces. The normal force is evaluated as function of the elastic pseudo-penetration depth between the impacting bodies, coupled with a nonlinear viscous-elastic factor representing the energy dissipation during the impact process. For this continuous contact force model, it is assumed that the compliance and damping coefficients are available.

An illustrative example and numerical results were presented, being the efficiency of the developed methodology discussed in the process of their presentation. In the application of the spatial four-bar mechanism, to demonstrate the formulation proposed, a spatial four-bar mechanism was used with a spherical clearance
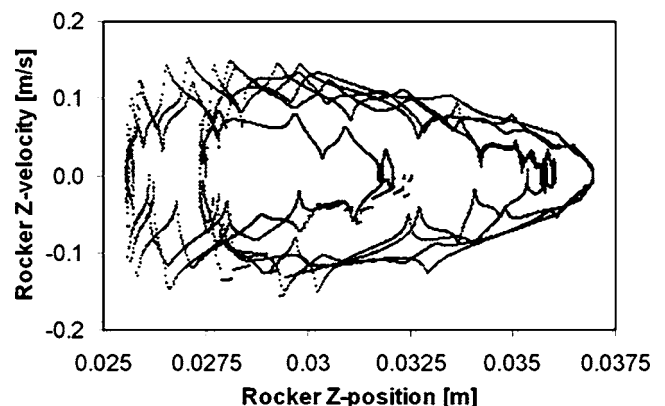

Fig. 18 Poincaré map: spherical clearance joint

joint formulation. The system was driven only by gravity, meaning that the system is not conservative in the presence of damping effects, and as a consequence, that some energy is dissipated in each cycle of the motion. The energy loss is shown to be much more important when a clearance joint is included into the system, due to the dissipative effect of the contact model used. This was clearly visible by comparing the position and velocity of the mechanical system to those of a system with ideal joints, meaning that the impacts within the clearance joint significantly increase the amount of dissipated energy.

The overall results presented in this work show that the introduction of clearance joints in spatial multibody mechanical systems significantly influences the prediction of components' position and drastically increase the peaks in acceleration and reaction moments at the joints. Moreover, the system's response clearly tends to be nonlinear when a clearance joint is included. This is a fundamental feature mainly in high speed and precision mechanisms where the accurate predictions are essential for the design of the mechanical systems.

Acknowledgment

References

[1] Dubowsky, S., and Freudenstein, F., 1971, "Dynamic Analysis of Mechanical Systems with Clearances, Part 1: Formulation of Dynamic Model," ASME J. Eng. Ind., **93**(1), pp. 305–309.

[2] Bahgat, B. M., Osman, M. O. M., and Sankar, T. S., 1979, "On the Effect of Bearing Clearances in the Dynamic Analysis of Planar Mechanisms," J. Mech. Eng. Sci., **21**(6), pp. 429–437.

[3] Seneviratne, L. D., and Earles, S. W. E., 1992, "Chaotic Behaviour Exhibited During Contact Loss in a Clearance Joint if a Four-Bar Mechanism," Mech. Mach. Theory, **27**(3), pp. 307–321.

[4] Farahanchi, F., and Shaw, S. W., 1994, "Chaotic and Periodic Dynamics of a Slider-Crank Mechanism with Slider Clearance," J. Sound Vib., **177**(3), pp. 307–324.

[5] Rhee, J., and Akay, A., 1996, "Dynamic Response of a Revolute Joint With Clearance," Mech. Mach. Theory, **31**(1), pp. 121–134.

[6] Flores, P., Ambrósio, J., and Claro, J. P., 2004, "Dynamic Analysis for Planar Multibody Mechanical Systems with Lubricated Joints," Multibody Syst. Dyn., **12**, pp. 47–74.

[7] Lankarani, H. M., and Nikravesh, P. E., 1990, "A Contact Force Model With Hysteresis Damping for Impact Analysis of Multibody Systems," ASME J. Mech. Des., **112**, pp. 369–376.

[8] Ambrósio, J. A. C., 2002, "Impact of Rigid and Flexible Multibody Systems: Deformation Description and Contact Models," *Virtual Nonlinear Multibody Systems*, NATO Advanced Study Institute, W. Schiehlen and M. Valásek, eds., Plenum, New York, Vol. II, pp. 15–33.

[9] Goldsmith, W., 1960, *Impact: The Theory and Physical Behaviour of Colliding Solids*, Edward Arnold Ltd, London.

[10] Nikravesh, P. E., 1988, *Computer-Aided Analysis of Mechanical Systems*, Prentice-Hall, Englewood Cliffs, NJ.

[11] Hertz, H., 1896, "On the Contact of Solids; On the Contact of Rigid Elastic Solids and on Hardness" translated by D. E. Jones and G. A. Schott, *Miscellaneous Papers*, Macmillan and Co. Ltd., London, pp. 146–183.

[12] Chang, C. O., and Nikravesh, P. E., 1985, "An Adaptive Constraint Violation Stabilization Method for Dynamic Analysis of Mechanical Systems," ASME J. Mech., Transm., Autom. Des., **107**, pp. 488–492.

[13] Baumgarte, J., 1972, "Stabilization of Constraints and Integrals of Motion in Dynamical Systems," Comput. Methods Appl. Mech. Eng., **1**, pp. 1–16.

[14] Shampine, L., and Gordon, M., 1975, *Computer Solution of Ordinary Differential Equations: The Initial Value Problem*, Freeman, San Francisco, CA.